

# Prototype for In Situ Detection of Atmospheric NO<sub>3</sub> and N<sub>2</sub>O<sub>5</sub> via Laser-Induced Fluorescence

EZRA C. WOOD,<sup>†</sup> PAUL J. WOOLDRIDGE,<sup>†</sup>  
JENS H. FREESE,<sup>†,‡</sup>  
TIM ALBRECHT,<sup>†,§</sup> AND  
RONALD C. COHEN\*<sup>†,||,⊥</sup>

Department of Chemistry and Department of Earth and Planetary Sciences, University of California, Berkeley, California 94720, and Energy and Environment Technologies Division, Lawrence Berkeley National Laboratory, 1 Cyclotron Road, Berkeley, California 94720

We describe a prototype designed for in situ detection of the nitrate radical (NO<sub>3</sub>) by laser-induced fluorescence (LIF) and of N<sub>2</sub>O<sub>5</sub> by thermal dissociation followed by LIF detection of NO<sub>3</sub>. An inexpensive 36 mW continuous wave multi-mode diode laser at 662 nm is used to excite NO<sub>3</sub> in the  $\tilde{B}^2E'(0000) \leftarrow \tilde{X}^2A_2'(0000)$  band. Fluorescence is collected from 700 to 750 nm. The prototype has a sensitivity to NO<sub>3</sub> of 76 ppt for a 60 s integration with an accuracy of 8%. Although this sensitivity is adequate for studies of N<sub>2</sub>O<sub>5</sub> in many environments, it is much less sensitive (about 300 times) than expected based on a comparison of previously measured photophysical properties of NO<sub>2</sub> and NO<sub>3</sub>. This implies much stronger nonradiative coupling of electronic states in NO<sub>3</sub> than in NO<sub>2</sub>.

## Introduction

In the earth's boundary layer, the nitrate radical (NO<sub>3</sub>) is an important oxidant and an intermediate in the conversion of NO<sub>x</sub> (NO<sub>x</sub> ≡ NO + NO<sub>2</sub>) to HNO<sub>3</sub>. NO<sub>3</sub> is formed by the reaction of NO<sub>2</sub> with O<sub>3</sub>. During the daytime, rapid photolysis ( $J = 0.2 \text{ s}^{-1}$ ) and reaction with NO limit concentrations to less than 1 ppt near the surface. In contrast, at night, when NO<sub>3</sub>, NO<sub>2</sub>, and N<sub>2</sub>O<sub>5</sub> are in equilibrium:



mixing ratios of NO<sub>3</sub> in the boundary layer have been measured in the range of 1–200 ppt (1). The few measurements above the boundary layer in the free troposphere indicated an average mixing ratio of 8 ppt (2), and stratospheric measurements have ranged from 5 to 160 ppt at altitudes of 22–38 km (3). There are few measurements of atmospheric N<sub>2</sub>O<sub>5</sub>. Brown et al. (4–7) and Simpson (8) are the only groups to measure N<sub>2</sub>O<sub>5</sub> in the troposphere, reporting

mixing ratios up to 3 ppb in the polluted continental boundary layer and up to 60 ppt at high latitudes. Stratospheric N<sub>2</sub>O<sub>5</sub>, with peak mixing ratios of 1.8 ppb, has been observed using spectrometers aboard balloons and satellites (9, 10).

Due to the equilibrium between NO<sub>3</sub> and N<sub>2</sub>O<sub>5</sub>, a loss of one species effectively constitutes a loss of the other. In the troposphere, NO<sub>3</sub> reacts rapidly with NO, alkenes, and dimethyl sulfide (1). In both the stratosphere and the troposphere, N<sub>2</sub>O<sub>5</sub> reacts with water in an efficient heterogeneous reaction to form HNO<sub>3</sub>. NO<sub>3</sub> also participates in heterogeneous reactions with water (11). In the troposphere, HNO<sub>3</sub> is usually removed by dry deposition or rainout faster than it is photochemically converted back to NO<sub>x</sub> and thus constitutes a permanent sink for NO<sub>x</sub>. In the stratosphere, where there is no rain, HNO<sub>3</sub> is a long-lived reservoir for NO<sub>x</sub>.

The most common method for measuring atmospheric NO<sub>3</sub> is differential optical absorption spectrometry (DOAS) across open path lengths on the order of 1 km. This remote sensing method utilizes a broadband light source and measures the differential absorption of light in the strong 662 nm absorption band ( $\sigma = 2.2 \times 10^{-17} \text{ cm}^2$ ) (12). A less commonly used method of detection is matrix-isolation electron spin resonance spectrometry (MI-ESR) (12), which involves cryogenically trapping whole air samples with subsequent laboratory analysis. Neither technique is adequate in its current form for routine use from aircraft, and laboratory throughput limits the use of MI-ESR to relatively infrequent sampling. Recently, Brown et al. (4–7) and Simpson (8) have demonstrated fast measurements of ambient NO<sub>3</sub> and N<sub>2</sub>O<sub>5</sub> via cavity ring-down spectroscopy (CaRDS). Their in situ approach allows for measurement of N<sub>2</sub>O<sub>5</sub> in the troposphere via heating of their inlet followed by detection of the NO<sub>3</sub> thermal dissociation product. Measurement of NO<sub>3</sub> in the laboratory using CaRDS has also been demonstrated (13, 14).

Although numerous studies of NO<sub>3</sub> and N<sub>2</sub>O<sub>5</sub> spectroscopy and kinetics have utilized laser-induced fluorescence (LIF) in the laboratory (15–20), LIF has not previously been applied to ambient detection of NO<sub>3</sub> and N<sub>2</sub>O<sub>5</sub>. In this paper, we describe a prototype for field measurements of NO<sub>3</sub> and N<sub>2</sub>O<sub>5</sub> using LIF.

## Laser-Induced Fluorescence Detection of NO<sub>3</sub>

LIF has proven to be an accurate, sensitive, and selective method for measurement of trace atmospheric species throughout the troposphere and stratosphere (21–24). A laser is used to excite the compound of interest to an excited electronic state, followed by measurement of the subsequent spontaneous emission (fluorescence). The advantages of this technique are the following:

(i) with careful cell design, the fluorescent light is detected against a very low background, which combined with photon-counting leads to high sensitivity;

(ii) high selectivity is achieved as the compound must meet the criteria of both absorbing the chosen excitation frequencies and emitting within a constrained spectroscopic window;

(iii) except at very low pressures, the fluorescence signal is proportional to the *mixing ratio* rather than number density as shown below, rendering the technique equally effective in the stratosphere and troposphere;

(iv) sampling can be accomplished with a minimum of surface contact.

\* Corresponding author phone: (510)642-2735; fax: (510)643-2156; e-mail: cohen@cchem.berkeley.edu.

<sup>†</sup> Department of Chemistry, University of California.

<sup>‡</sup> Present address: Optical Institute, Technische Universität, Berlin, Germany.

<sup>§</sup> Present address: Technische Universität Berlin, Max-Volmer-Institut für Biophysikalische Chemie und Biochemie, Berlin, Germany.

<sup>||</sup> Department of Earth and Planetary Sciences, University of California.

<sup>⊥</sup> Lawrence Berkeley National Laboratory.

The signal rate  $S$  (photon counts/s) observed during LIF is given by the following expression:

$$S = E \times Q \times C \quad (2)$$

where  $E$  is the excitation rate,  $Q$  is the fluorescence quantum yield, and  $C$  is the collection efficiency of the instrument. These three quantities can be calculated and used to estimate the calibration constant of an LIF instrument. However, the calibration constant of our instrument is *not* determined by the calculation of these quantities but rather by the introduction of a known concentration of  $\text{NO}_3$ . The excitation rate is

$$E = cI \int \phi(\nu)\sigma(\nu, \text{temperature}) \, d\nu \quad (3)$$

where  $c$  is the number density of the excited species,  $I$  is the excited path length, and the integral represents the overlap between the laser line shape  $\phi(\nu)$  and the absorption cross section of the molecule,  $\sigma(\nu, \text{temperature})$ .

The fluorescence quantum yield ( $Q$ ) is the fraction of excited molecules which fluoresce [i.e., (photons emitted)/(photons absorbed)]. For a two-state system, the fluorescence quantum yield is given by

$$Q = \frac{k_f}{k_f + k_{IC} + \sum_i k_{qi}[M_i]} \quad (4)$$

where  $k_f$  is the fluorescence rate constant of the excited species,  $k_{IC}$  is the rate constant of nonradiative internal conversion, and  $\sum k_{qi}$  are the fluorescence quenching rate constants due to collisional deactivation by bath molecules  $M_i$ . The sum of  $k_f$  and  $k_{IC}$  is the observed radiative decay rate constant [i.e., the reciprocal excited-state lifetime ( $1/\tau_0$ )]. For the condition that  $\sum k_{qi}[M_i]$  is much greater than the first two terms of the denominator, the  $1/[M]$  term in the fluorescence quantum yield will combine with the  $c$  term in the excitation rate to make the overall signal rate proportional to  $c/[M]$ , which is the mixing ratio. This allows the detection cell to be held at lower than ambient pressure without a penalty in the signal rate, which reduces pressure-dependent noise sources (e.g., Raman and Rayleigh scattering). For molecules such as  $\text{NO}_2$  and  $\text{NO}_3$ , which have anomalously long fluorescence lifetimes, the condition that the  $\sum k_{qi}[M_i]$  term dominates is satisfied even at pressures lower than 5 Torr.

The collection efficiency ( $C$ ) is given by

$$C = \Omega \times T \times \epsilon \times F \quad (5)$$

where  $\Omega$  is the fraction of the solid angle of the fluorescence intercepted by the collection optics,  $T$  is the transmission of the optics,  $\epsilon$  is the fraction of fluorescence that occurs within the active spectral region of the PMT, and  $F$  is the fraction of the fluorescence that occurs in the time gate of a pulsed detection system.  $\epsilon$  contains information on the fluorescing molecule's emission spectrum and on the quantum efficiency of the PMT. The product  $T \times \epsilon$  is the fraction of the emission spectrum that is transmitted through the filters and detected by the PMT.

The absorption and fluorescence spectra of  $\text{NO}_3$  and its dissociation dynamics have been studied in detail (15, 17–20, 25–27). The  $\text{NO}_3$  absorption spectrum is broad and diffuse, with no rotational structure evident even under high resolution (28, 29). Like  $\text{NO}_2$ , the excited-state lifetime of  $\text{NO}_3$  is over 2 orders of magnitude longer than the lifetime calculated from its absorption cross section. These properties have been explained in the context of the Douglas effect (i.e., strong coupling between the ground and excited electronic states) (30). For  $\text{NO}_3$ , the  $\tilde{\text{B}}^2\text{E}'$  electronic state is strongly

perturbed by high-lying rovibrational states of the  $\tilde{\text{X}}^2\text{A}_2'$  and possibly the  $\tilde{\text{A}}^2\text{E}''$  electronic states (15, 19, 29–31). Thus, the broad 0–0 band at 662 nm is not an excitation to an isolated rovibronic state; rather it is to a manifold of isoenergetic  $^2\text{A}_2'$  states,  $^2\text{E}'$  states, and possibly  $^2\text{E}''$  states. The radiative rate has been shown to be biexponential, and there is considerable uncertainty in the relative magnitudes of the fast and slow components of the excited-state radiative decay. Nelson et al. (18) examined the 0–0 band at 662 nm and measured an excited-state lifetime [ $\tau = (k_f + k_{IC})^{-1}$ ] of 340  $\mu\text{s}$  for the slow component of the decay and an air-average fluorescence quenching rate constant of  $1.8 \times 10^{-11} \text{ cm}^3 \text{ molecules}^{-1} \text{ s}^{-1}$ . Carter et al. (15) observed a biexponential decay with a fast component of roughly 30  $\mu\text{s}$  in a sample of jet-cooled ( $T_{\text{rotational}} = 2\text{--}3 \text{ K}$ )  $\text{NO}_3$ . Ishiwata et al. (17) observed a single-exponential decay for the excited state and measured a lifetime of 2.8  $\mu\text{s}$ , although it appears that they may not have measured the fluorescence decay for long enough and/or may have operated at pressures too high to observe the slow component.

Given these uncertainties and the difficulty of directly calculating fluorescence quantum yields, it is useful to use  $\text{NO}_2$  as a benchmark for estimating the potential of LIF for  $\text{NO}_3$  detection since we have extensive experience with detection of ambient  $\text{NO}_2$  by LIF (21, 24, 32). Our most sensitive  $\text{NO}_2$  LIF instrument utilizes a pulsed dye laser at 585 nm and has a signal rate of 0.5 counts  $\text{s}^{-1} \text{ ppb}^{-1} \text{ mW}^{-1}$ . In Table 1, we compare the parameters describing  $\text{NO}_3$  and  $\text{NO}_2$  detection by LIF. The ratio of excitation rates  $E_{\text{NO}_3}/E_{\text{NO}_2}$  (eq 3) is 400 due to the higher absorption cross section of  $\text{NO}_3$  at 662 nm as compared to that of  $\text{NO}_2$  at 585 nm. The product ( $T \times \epsilon$ ) is much lower for  $\text{NO}_2$  than for  $\text{NO}_3$  as most of  $\text{NO}_2$  fluorescence occurs in the near-IR (37, 38) and therefore outside the active spectral region of efficient red-sensitive photomultiplier tubes, whereas  $\text{NO}_3$  fluoresces almost entirely in the visible. We estimate that only  $\sim 8\%$  of the full spectral range of  $\text{NO}_2$  fluorescence is collected within the spectral window of our  $\text{NO}_2$  instrument (700–850 nm), whereas 50% of  $\text{NO}_3$  fluorescence is collected within a spectral window of 700–750 nm for an  $\text{NO}_3$  instrument. The fraction of fluorescence that occurs in the instrument's temporal window ( $F$ ) is 1 for cw excitation of  $\text{NO}_3$  and  $\sim 0.8$  for the time gates used by our  $\text{NO}_2$  LIF instrument. Thus the ratio  $(T\epsilon F)_{\text{NO}_3, 662\text{nm}}/(T\epsilon F)_{\text{NO}_2, 585\text{nm}}$  is approximately  $(0.5 \times 1)/(0.08 \times 0.8) = 8$ . Assuming equal fluorescence quantum yields and geometric collection efficiencies ( $\Omega$ ) for  $\text{NO}_3$  and  $\text{NO}_2$ , one would predict a signal rate for  $\text{NO}_3$  of 0.5 counts  $\text{s}^{-1} \text{ ppb}^{-1} \text{ mW}^{-1} \times 400 \times 8 = 1600 \text{ counts s}^{-1} \text{ ppb}^{-1} \text{ mW}^{-1}$ , which combined with 36 mW of laser power and a background of 1500 counts/s would lead to a detection limit of 0.3 ppt with 60 s averaging as calculated in the detection limit section below.

We designed an LIF system for  $\text{NO}_3$  detection based on this analysis. Light from a 36 mW, cw multi-mode 662 nm InAlGaP laser diode enters a 40-pass Herriott cell perpendicular to the gas flow and induces excitation in the  $\tilde{\text{B}}^2\text{E}'(0000) \leftarrow \tilde{\text{X}}^2\text{A}_2'(0000)$  band of  $\text{NO}_3$  (Figure 1). The bandwidth of the 662 nm laser is 0.4 nm and is coarsely tuned by adjustment of the diode temperature and current. Fluorescence is measured orthogonal to the gas flow and laser axes. A fraction of the fluorescence is collected and collimated by a 55 mm focal length lens mounted above the laser beam. A concave mirror (40 mm radius of curvature) sits below the laser beam and increases the fluorescence signal by 80%. The fluorescence then sequentially passes through a 700 nm long-pass filter and a 750 nm short-pass filter and is then focused onto the photocathode of a thermoelectrically cooled red-sensitive GaAs Hamamatsu H7421-50 photomultiplier tube (PMT) equipped with an internal preamplifier and discriminator. These filters transmit slightly less than half of the total

TABLE 1. Relevant Parameters for Comparison of NO<sub>2</sub> LIF and NO<sub>3</sub> LIF

parameter	NO <sub>2</sub>	NO <sub>3</sub>
absorption cross-section ( $\sigma$ )	$5.5 \times 10^{-20} \text{ cm}^2$ at 585 nm (33)	$2.2 \times 10^{-17} \text{ cm}^2$ at 662 nm (34)
radiative lifetime ( $\tau = k_r^{-1}$ )	$\sim 100 \mu\text{s}$ (35)	biexponential; 3–30 $\mu\text{s}$ short, 340 $\mu\text{s}$ long (17, 18)
air-average fluorescence quenching rate coeff ( $k_q$ )	$6 \times 10^{-11} \text{ cm}^3 \text{ molecule}^{-1} \text{ s}^{-1}$ (36)	$1.8 \times 10^{-11} \text{ cm}^3 \text{ molecule}^{-1} \text{ s}^{-1}$ (18)
fraction of emission spectrum detected by PMT ( $T \times \epsilon$ )	8%	50%
fraction of fluorescence collected by time gate ( $F$ )	0.8	1
sensitivity	0.5 counts $\text{s}^{-1} \text{ ppb}^{-1} \text{ mW}^{-1}$	1600 counts $\text{s}^{-1} \text{ ppb}^{-1} \text{ mW}^{-1}$ predicted 4.9 counts $\text{s}^{-1} \text{ ppb}^{-1} \text{ mW}$ observed <sup>a</sup>

<sup>a</sup> See text for details.

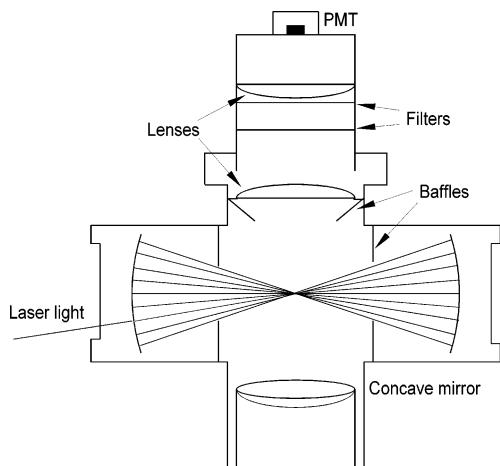


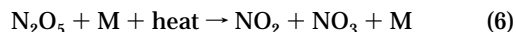
FIGURE 1. Detection cell. Gas flow is orthogonal to the page. The entrance windows are uncoated. The beam diameter in the center of the cell is approximately 0.5 mm.

fluorescence from NO<sub>3</sub> (20, 31) while rejecting most of the fluorescence stemming from NO<sub>2</sub> and greatly reducing the nonresonant background. Pulses from the PMT are counted by a multi-function data acquisition board. Laser scatter and light leaks (e.g., solar scatter) are minimized by use of highly reflective mirrors, by geometric baffling of stray light, and by coating the interior of the detection cell with a black optical paint. The number of passes (40) the laser beam makes in the Herriott cell was found to be a good balance between the favorable increase in laser fluence in the detection cell and the unfavorable increase in scattered light.

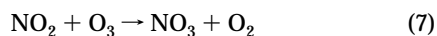
To confirm that the signal was indeed produced by NO<sub>3</sub> fluorescence, we measured the excitation spectrum of the calibration gas mixture by tuning the multi-mode diode laser from 659 to 663 nm and monitoring the fluorescence. The excitation spectrum is shown in Figure 2 along with the absorption cross section for reference.

### Calibration

The instrument is calibrated (Figure 3) using NO<sub>3</sub> produced by the thermal dissociation of N<sub>2</sub>O<sub>5</sub>(g):



N<sub>2</sub>O<sub>5</sub>(g) is produced by mixing gaseous NO<sub>2</sub> and O<sub>3</sub> with NO<sub>2</sub> in stoichiometric excess:



Ozone is produced by photolysis of zero air at 185 nm using a mercury lamp and quantified using the 254 nm line of a second mercury lamp. Typically, 14 ppm of N<sub>2</sub>O<sub>5</sub> is synthesized and diluted to 50–500 ppb before it is thermally

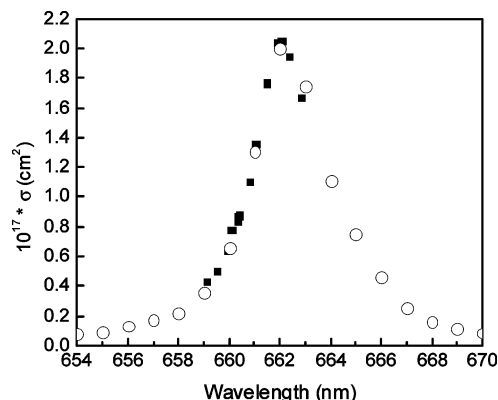
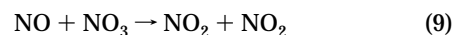


FIGURE 2. Excitation spectrum of 250 ppb NO<sub>3</sub> (solid squares), recorded by coarsely tuning the multi-mode diode laser over its tuning range via temperature control. Ref 39 recommended absorption cross section values (open circles) shown for reference. The fluorescence was normalized to laser power.

dissociated in a 20 cm long, 4 cm i.d. uncoated glass tube. The tube is externally heated to 120 °C and held at 9 Torr. Typical residence times in the tube were 300 ms—more than 13 times the lifetime for N<sub>2</sub>O<sub>5</sub> dissociation (22 ms; 39).

To quantify the NO<sub>3</sub>, it is converted to NO<sub>2</sub> by reaction with NO. A flow of 3 standard cubic centimeters/min (sccm) of 3% NO in N<sub>2</sub> (Matheson Tri-gases) is injected into the end of the flow tube. Reaction with NO rapidly converts the NO<sub>3</sub> into NO<sub>2</sub>:



The NO is flowed through an FeSO<sub>4</sub> trap before use in order to reduce any NO<sub>2</sub> impurity to NO. High concentrations of NO are used ( $\sim 5 \times 10^{13} \text{ molecules/cm}^3$ ) so that the pseudo-first-order rate constant for reaction 9 is extremely high:  $k_9[\text{NO}] > 1000 \text{ s}^{-1}$ . As the N<sub>2</sub>O<sub>5</sub> was prepared with NO<sub>2</sub> in excess, complications arising from the much slower reaction NO + O<sub>3</sub> are minimal. Light from a 7 mW, InAlGaP tunable diode laser (TUI optics) at 638 nm is used to detect the NO<sub>2</sub>. The laser frequency is continuously tuned on and off a single rovibronic feature in the absorption spectrum of NO<sub>2</sub>, thus modulating the fluorescence that stems from NO<sub>2</sub>. In addition to inducing NO<sub>2</sub> fluorescence, the 638 nm light also excites the  $\tilde{\text{B}}^2\text{E}'(1000) \leftarrow \tilde{\text{X}}^2\text{A}'_2(0001)$  transition of NO<sub>3</sub>. As the NO<sub>3</sub> absorption spectrum is diffuse and shows no rotational structure even under high resolution, the amount of fluorescence stemming from NO<sub>3</sub> does not change with the small shift in laser frequency (0.2  $\text{cm}^{-1}$ ) as it is tuned on and off the NO<sub>2</sub> absorption feature. This enables the NO<sub>3</sub> fluorescence to be distinguished from the NO<sub>2</sub> fluorescence. Although this NO<sub>3</sub> fluorescence is not quantitatively used for the calibration, it is useful for confirming the presence of NO<sub>3</sub> and in determining the amount of NO to add during the calibration. The 750 nm short-pass filter is removed while

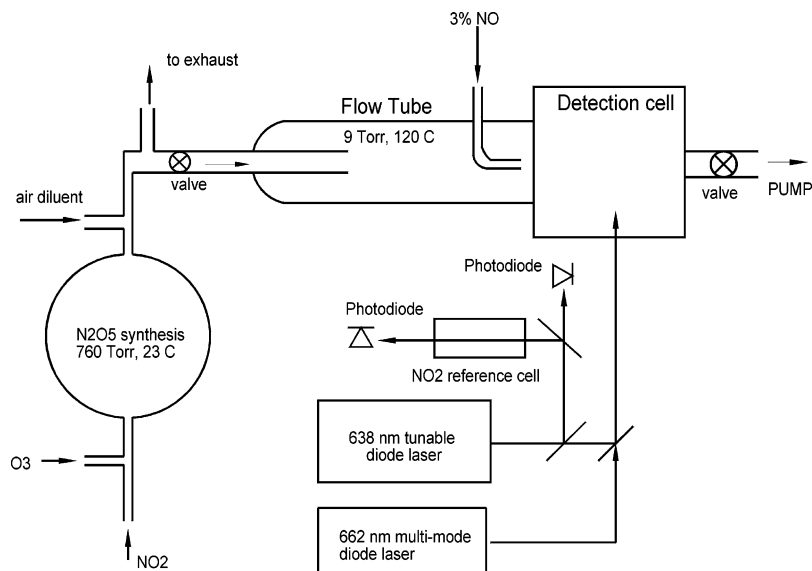


FIGURE 3. Experimental setup for calibrations.  $\text{N}_2\text{O}_5(\text{g})$  is synthesized in a 1 L flask and thermally dissociated in a Pyrex flow tube at 9 Torr and 120 °C. Light from one of two lasers enters the detection cell for LIF of  $\text{NO}_2$  and  $\text{NO}_3$ .

the 638 nm tunable laser light enters the cell in order to maximize the collection of  $\text{NO}_2$  fluorescence.

Three steps are required to obtain each point on the  $\text{NO}_3$  calibration curve:

(step A)  $\text{NO}_3$  response:  $\text{N}_2\text{O}_5$  is thermally dissociated in the flow tube, producing a mixture of  $\text{NO}_2$  and  $\text{NO}_3$  in the detection cell. The 662 nm laser light is directed into the detection cell and the  $\text{NO}_3$  fluorescence is measured.

(step B)  $\text{NO}_2$  quantification: with the same flow as above, the  $\text{NO}_2$  mixing ratio is quantified by  $\text{NO}_2$  LIF using the tunable diode laser at 638 nm.

(step C)  $\text{NO}_3$  quantification:  $\text{NO}$  is added to the  $\text{NO}_2 + \text{NO}_3$  mixture at the end of the flow tube. This rapidly converts the  $\text{NO}_3$  into  $\text{NO}_2$ , which is measured by LIF at 638 nm.

A wall loss rate ( $k_w$ ) of  $0.1 \text{ s}^{-1}$  at 413 K was measured by mixing  $\text{NO}_2$  with excess  $\text{O}_3$  in a longer flow tube of the same material as the one used for the calibration. The simplified reaction scheme below (eqs 10 and 11) was assumed, and the  $\text{NO}_2$  and  $\text{NO}_3$  fluorescence signals were observed over a range of reaction times:



$$[\text{NO}_3](t) = \frac{k_1[\text{NO}_2]_0}{k_1 - k_w} (e^{-k_w t} - e^{-k_1 t}) \quad (11)$$

The wall loss rate constant was determined by fitting the  $\text{NO}_3$  fluorescence data to the form of eq 11. A wall loss rate constant of  $0.1 \text{ s}^{-1}$  implies a loss of  $<0.2\%$  during the 20 ms between the  $\text{NO}$  injection point and the LIF detection point.

Figure 4 depicts typical calibration data. The  $\text{NO}_3$  mixing ratio is calculated in step C as half the difference in  $\text{NO}_2$  mixing ratio with and without added  $\text{NO}$ :

$$[\text{NO}_3] = 0.5 \{ [\text{NO}_2]_{(\text{step C})} - [\text{NO}_2]_{(\text{step B})} \} \quad (12)$$

The factor of 0.5 accounts for the stoichiometry of reaction 9. Figure 5 is a calibration curve for LIF at 9 Torr and 393 K. The instrument's calibration constant is the slope of the line  $3.8 \pm 0.3 \text{ counts s}^{-1} \text{ ppb}^{-1} \text{ mW}^{-1}$ . The source of the uncertainty is that  $[\text{NO}_2]_{(\text{step C})}$  and  $[\text{NO}_2]_{(\text{step B})}$  are both determined by calculating the difference between "online" and "offline" count rates. These uncertainties, when propagated through to the calibration constant, result in an overall  $\pm 8\%$  uncertainty.

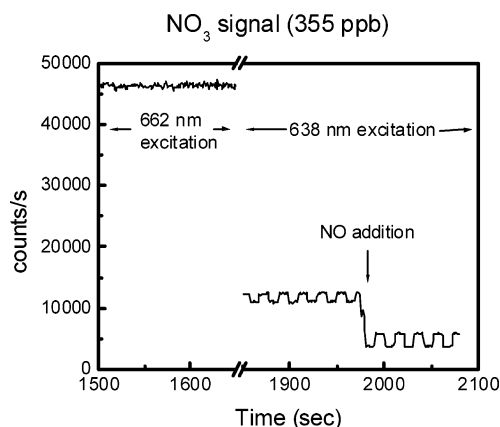


FIGURE 4. Calibration data. A mixture of  $\text{NO}_2$  and  $\text{NO}_3$  is flowing into the detection cell. From time = 1500–1650 s, the fluorescence signal induced by 662 nm excitation of the  $\text{NO}_3$  is measured (step A). From time = 1850–1970 s, the 638 nm tunable diode laser is used to quantify the  $\text{NO}_2$  concentration (step B). The total signal at this point is the sum of constant  $\text{NO}_3$  fluorescence and modulating on-line and off-line  $\text{NO}_2$  fluorescence. At time = 1970 s,  $\text{NO}$  is added to the calibration gas, converting the  $\text{NO}_3$  into  $\text{NO}_2$  (step C). The  $\text{NO}_3$  concentration is calculated by the increase in  $\text{NO}_2$  concentration.

The absorption cross section of the 0–0 band at 662 nm increases with decreasing temperature due to the increased population of the ground vibrational state (27, 34). We estimate that the sensitivity to  $\text{NO}_3$  is 30% higher at 298 K than at 393 K based on the Boltzmann distribution in  $\nu = (0000)$ . Thus the instrument calibration constant at 298 K is  $4.9 \text{ counts s}^{-1} \text{ ppb}^{-1} \text{ mW}^{-1}$ .

This calibration constant is over 300 times lower than expected ( $1600 \text{ counts s}^{-1} \text{ ppb}^{-1} \text{ mW}^{-1}$ ) based on the approximations shown in Table 1 and indicates a major flaw in the approximation of equal fluorescence quantum yields for  $\text{NO}_3$  and  $\text{NO}_2$ . As the radiative lifetimes and fluorescence quenching rate constants of  $\text{NO}_2$  and  $\text{NO}_3$  are comparable, we attribute this large difference in fluorescence quantum yield to the relative rates of internal conversion of the two species. The 0–0 band at 662 nm is an excitation to a manifold of states with only partial  ${}^2E'$  (bright) character as the  $\tilde{B}^2E'$  state of  $\text{NO}_3$  is strongly perturbed by high-lying rovibrational levels of the  $\tilde{X}^2A_2'$  ground state. Although the excited state

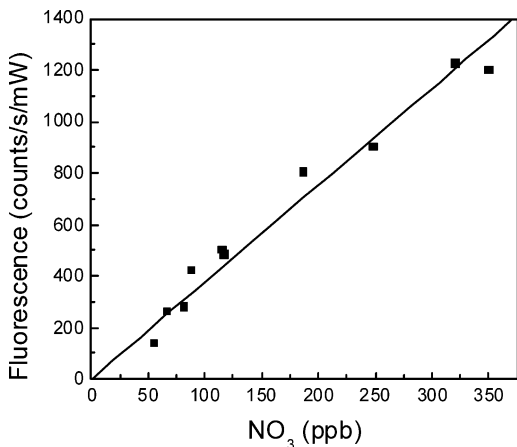


FIGURE 5. Calibration curve for  $\text{NO}_3$  at  $120^\circ\text{C}$ . The slope =  $3.8 \pm 0.3 \text{ counts s}^{-1} \text{ ppb}^{-1} \text{ mW}^{-1}$ .

of  $\text{NO}_2$  ( $\tilde{A}^2B_2$ ) is also perturbed by high-lying rovibrational levels of its ground state ( $\tilde{X}^2A_1$ ), the density of states of  $\text{NO}_2$  near  $662 \text{ nm}$  is 2–3 orders of magnitude less than that of  $\text{NO}_3$  (15, 19, 40). Thus the potential for radiationless decay is substantially greater for  $\text{NO}_3$ . Uncertainty in the  $\text{NO}_3$  fluorescence decay rate does not simply explain the difference in fluorescence quantum yield. Use of a higher value of  $k_f$  in eq 4 ( $2.8 \mu\text{s}$  instead of  $340 \mu\text{s}$ ) for  $\text{NO}_3$  corresponding to its fast component of biexponential fluorescence would only produce an even bigger discrepancy between the predicted and observed calibration constants, and use of a slower value of  $k_f$  would correspond to an unrealistically long fluorescence lifetime, much greater than measured in the literature (15, 17, 18). The fluorescence signal was linear with laser power, indicating that the transition was not saturated.

**Sensitivity.** The detection limit is determined by the instrument's sensitivity to  $\text{NO}_3$  and by the background signal. At  $36 \text{ mW}$ , the calibration constant  $\alpha$  was measured to be  $176 \text{ counts s}^{-1} \text{ ppb}^{-1}$ . The background signal consists of two parts: (i) the instrumental background, measured with zero air flowing in the detection cell; and (ii) the fluorescence from other chemical species, of which the only important term is  $\text{NO}_2$ . The instrumental background at  $36 \text{ mW}$  is  $1340 \text{ counts/s}$ . Of these  $1340 \text{ counts/s}$ , 25 are PMT dark counts, 560 are oxygen Raman scattering, and the remainder are laser scatter. The  $\text{NO}_2$  fluorescence rate at  $662 \text{ nm}$  is  $0.14 \text{ counts s}^{-1} \text{ ppb}^{-1}$ . For  $10 \text{ ppb}$  of  $\text{NO}_2$ , this corresponds to  $1.4 \text{ counts/s}$ .

The observed mixing ratio in ppb ( $\chi$ ) is  $S_{\text{LIF}}/\alpha$  where  $S_{\text{LIF}}$  is the LIF signal in counts/s and  $\alpha$  is the instrument's calibration constant in  $\text{counts s}^{-1} \text{ ppb}^{-1}$ .  $S_{\text{LIF}}$  is determined by subtracting the background count rate,  $B$  (counts/s), from the total count rate  $S_{\text{LIF}} + B$ . The associated uncertainty ( $\sigma_S$ ) with this subtraction is given by

$$\sigma_S = \sqrt{(\sigma_{S+B})^2 + \sigma_B^2} \quad (13)$$

where  $\sigma_{S+B}$  and  $\sigma_B$  are the uncertainties of the total count rate and background count rates, respectively. The signal-to-noise ratio (SNR) with an integration time ( $t$ ) is then

$$\text{SNR} = \frac{S_{\text{LIF}}t}{\sigma_S} = \frac{S_{\text{LIF}}t}{\sqrt{S_{\text{LIF}}t + 2Bt}} \quad (14)$$

At the detection limit,  $S_{\text{LIF}} \ll 2B$ . Rearranging eq 14 gives the minimum detectable mixing ratio ( $\chi_{\text{min}}$ ) of

$$\chi_{\text{min}} = \frac{\text{SNR}}{\alpha} \sqrt{\frac{2B}{t}} \quad (15)$$

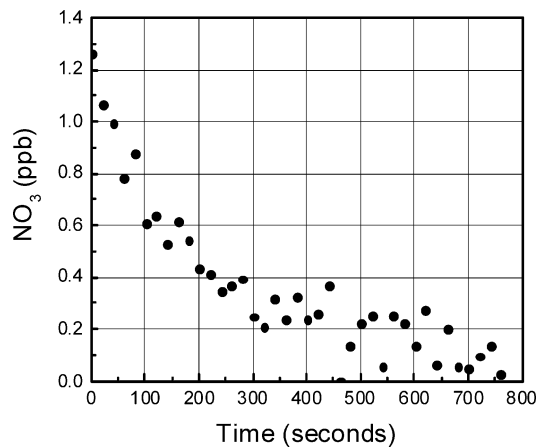


FIGURE 6. 20-s averages for a decaying  $\text{NO}_3$  source. The magnitude of the noise ( $1\sigma = 0.1 \text{ ppb}$ ) is evident.

This calculation assumes that the uncertainty in the instrument zero is negligible.

At  $\text{SNR} = 2$ , with  $36 \text{ mW}$  of laser power and at an  $\text{NO}_2$  concentration of  $10 \text{ ppb}$ , this yields a detection limit of  $76 \text{ ppt}$  for a  $60 \text{ s}$  average at  $298 \text{ K}$ . Although this detection limit is not sufficient for measurement of  $\text{NO}_3$  as ambient mixing ratios are rarely this high, it is sufficient for measurement of  $\text{N}_2\text{O}_5$  in most environments. This sensitivity is reflected in Figure 6 in the measurements of  $\text{NO}_3$  from a sample that is being increasingly diluted.

**Prospects for Field Measurements.** Adaptation of the prototype for field measurement of ambient  $\text{N}_2\text{O}_5$  will require only a few modifications. Foremost is the development of an inlet, which must be able to rapidly thermally dissociate  $\text{N}_2\text{O}_5$  and create a pressure drop with a minimum of surface contact. The inlet design would consist of a short heating section (e.g.,  $5 \text{ ms}$  at  $150^\circ\text{C}$  and  $1 \text{ atm}$ ) followed by an expansion through an orifice similar to those used by tropospheric OHLIF instruments (22, 41–44). The instrument including its inlet would be calibrated in the laboratory as above. An absolute calibration in the field would be unnecessary since the ratio of the instrument's  $\text{NO}_3$  LIF calibration constant to both the instrument's  $\text{NO}_2$  LIF sensitivity and to its air Raman scattering sensitivity are constants. As long as these two ratios are accurately measured in the laboratory, these two diagnostics, which do not require as much equipment and are not as time-consuming as  $\text{NO}_3$  calibrations, can serve as proxies for an absolute  $\text{NO}_3$  calibration and can quantify drifts in the instrument's calibration constant during a field deployment. As the Raman sensitivity can be measured very precisely, use of this proxy calibration would only minimally affect the uncertainty of the absolute  $\text{NO}_3$  calibration constant. Use of Raman or Rayleigh signal as a transfer standard for calibrations has been applied to OH,  $\text{NO}_2$ , ClO, and BrO measurements (21, 23, 45–47).

In the CaRDS system used by Brown et al., a Nd:YAG-pumped dye laser ( $60 \text{ mW}$ ) is used to attain a sensitivity of  $0.25 \text{ ppt}$  in  $5 \text{ s}$ . Their precision on time scales of minutes to hours is limited primarily by their need to sample through a Teflon membrane filter in order to reduce the effects of aerosol extinction on the observed ring-down time, resulting in an uncertainty of  $10\text{--}20\%$  depending on the exposure time of the filter in use. The rest of their inlet is coated with a halocarbon wax to reduce wall losses. The use of filters results in a requirement for frequent ( $1\text{--}3 \text{ h}$ ) maintenance to limit losses of  $\text{NO}_3$  as the filters become dirty. Although our LIF prototype is less sensitive than CaRDS for  $\text{NO}_3$ , it will potentially be simpler to operate and maintain and has the advantage that ambient air can be sampled with a minimum

of surface contact as no filters are required. Additionally, LIF is well-suited for use in the stratosphere as the signal per mixing ratio is invariant with ambient pressure and an extremely small package could be assembled for aircraft or balloon-borne measurements.

Detection of ambient NO<sub>3</sub> via LIF requires the background be significantly reduced and the signal rate increased from the prototype described above. Use of a pulsed laser with time-gated photon counting would greatly reduce the background. An instrument with 100 mW average power and a background of 2 counts/s would have a detection limit of 1 ppt with a 60 s integration. The NO<sub>2</sub> fluorescence signal will likely be comparable to the NO<sub>3</sub> fluorescence signal at low NO<sub>3</sub> mixing ratios, making it difficult to achieve such a low background count rate. Concurrent independent measurements of NO<sub>2</sub> taken alongside NO<sub>3</sub> and N<sub>2</sub>O<sub>5</sub> measurements can be used to quantify this component of the background.

In summary, we have built a prototype for detection of NO<sub>3</sub> and N<sub>2</sub>O<sub>5</sub> via thermal dissociation—LIF—using a simple inexpensive 662 nm cw diode laser. The current detection limit at 298 K of 76 ppt with a 60 s integration is adequate for observing ambient N<sub>2</sub>O<sub>5</sub>, and offers the potential for portable measurements of this species throughout the troposphere and stratosphere. Field measurements with this prototype are planned for Fall 2003.

### Acknowledgments

This work was supported by NSF Grant 0138669. J.H.F. and T.A. acknowledge support from the German National Merit Foundation (Studienstiftung des Deutschen Volkes). Early work on this project was supported by the NASA Instrument Incubator Program under Contract NAS1-99053.

### Literature Cited

- Platt, U.; Heintz, F. Nitrate Radicals in Tropospheric Chemistry. *Isr. J. Chem.* **1994**, *34* (3–4), 289–300.
- Carslaw, N.; et al. Observations of the nitrate radical in the free troposphere at Izana de Tenerife. *J. Geophys. Res.* **1997**, *102* (D9), 10613–10622.
- Naudet, J. P.; et al. Altitude distribution of stratospheric NO<sub>3</sub>: I. Observations of NO<sub>3</sub> and related species. *J. Geophys. Res.* **1989**, *94*, 6374–6382.
- Brown, S. S.; et al. In-situ measurement of atmospheric NO<sub>3</sub> and N<sub>2</sub>O<sub>5</sub> via cavity ring-down spectroscopy. *Geophys. Res. Lett.* **2001**, *28* (17), 3227–3230.
- Brown, S. S.; Stark, H.; Ravishankara, A. R. Cavity ring-down spectroscopy for atmospheric trace gas detection: application to the nitrate radical (NO<sub>3</sub>). *Appl. Phys. B: Lasers Opt.* **2002**, *75* (2–3), 173–182.
- Brown, S. S.; et al. Simultaneous in situ detection of atmospheric NO<sub>3</sub> and N<sub>2</sub>O<sub>5</sub> via cavity ring-down spectroscopy. *Rev. Sci. Instrum.* **2002**, *73* (9), 3291–3301.
- Brown, S. B.; et al. Nitrogen oxides in the nocturnal boundary layer: Simultaneous in situ measurements of NO<sub>3</sub>, N<sub>2</sub>O<sub>5</sub>, NO<sub>2</sub>, NO, and O<sub>3</sub>. *J. Geophys. Res. Atmos.* **2003**, *108* (D9).
- Simpson, W. R. Continuous wave cavity ring-down spectroscopy applied to in situ detection of dinitrogen pentoxide (N<sub>2</sub>O<sub>5</sub>). *Rev. Sci. Instrum.* **2003**, *74* (7), 3442–3452.
- Kunde, V. G.; et al. Measurement of nighttime stratospheric N<sub>2</sub>O<sub>5</sub> from infrared emission spectra. *Geophys. Res. Lett.* **1988**, *15*, 1177–1180.
- Toon, G. C.; Farmer, C. B.; Norton, R. H. Detection of stratospheric N<sub>2</sub>O<sub>5</sub> by infrared remote sounding. *Nature* **1986**, *319*, 570–571.
- Rudich, Y.; Talukdar, R. K.; Ravishankara, A. R. Multiphase chemistry of NO<sub>3</sub> in the remote troposphere. *J. Geophys. Res.* **1998**, *103* (D13), 16133–16143.
- Geyer, A.; et al. Comparison of tropospheric NO<sub>3</sub> radical measurements by differential optical absorption spectroscopy and matrix isolation electron spin resonance. *J. Geophys. Res. [Atmos.]* **1999**, *104* (D21), 26097–26105.
- Ball, S. M.; et al. Broadband cavity ringdown spectroscopy of the NO<sub>3</sub> radical. *Chem. Phys. Lett.* **2001**, *342*, 113–120.
- King, M. D.; Dick, E. M.; Simpson, W. R. A new method for the atmospheric detection of the nitrate radical (NO<sub>3</sub>). *Atmos. Environ.* **2000**, *34*, 685–688.
- Carter, R. T.; et al. A high-resolution study of the NO<sub>3</sub> radical produced in a supersonic jet. *Chem. Phys. Lett.* **1996**, *257* (3–4), 297–302.
- Hammer, P. D.; Dlugokencky, E. J.; Howard, C. J. Kinetics of the Gas-Phase Reaction NO + NO<sub>3</sub> → 2NO<sub>2</sub>. *J. Phys. Chem.* **1986**, *90*, 2491–2496.
- Ishiwata, T.; et al. Study of NO<sub>3</sub> by laser-induced fluorescence. *J. Phys. Chem.* **1983**, *87* (8), 1349–1352.
- Nelson, H. H.; Pasternack, L.; McDonald, J. R. Excited-state dynamics of NO<sub>3</sub>. *J. Chem. Phys.* **1983**, *79* (9), 4279–4284.
- Mikhailichenko, K.; et al. Unimolecular decomposition of NO<sub>3</sub>: the NO+O<sub>2</sub> threshold regime. *J. Chem. Phys.* **1996**, *105* (16), 6807–6817.
- Kim, B. S.; Hunter, P. L.; Johnston, H. S. NO<sub>3</sub> Radical Studied By Laser-Induced Fluorescence. *J. Chem. Phys.* **1992**, *96* (6), 4057–4067.
- Thornton, J. A.; Wooldridge, P. J.; Cohen, R. C. Atmospheric NO<sub>2</sub>: In situ laser-induced fluorescence detection at parts per trillion mixing ratios. *Anal. Chem.* **2000**, *72* (3), 528–539.
- Stevens, P. S.; Mather, J. H.; Brune, W. H. Measurement of tropospheric OH and HO<sub>2</sub> by laser-induced fluorescence at low pressure. *J. Geophys. Res.* **1994**, *99* (D2), 3543–3557.
- Wennberg, P. O.; et al. Aircraft-borne, laser-induced fluorescence instrument for the in-situ detection of hydroxyl and hydroperoxyl radicals. *Rev. Sci. Instrum.* **1994**, *65* (6), 1858–1876.
- Day, D. A.; et al. A thermal dissociation laser-induced fluorescence instrument for in situ detection of NO<sub>2</sub>, peroxy nitrates, alkyl nitrates, and HNO<sub>3</sub>. *J. Geophys. Res. [Atmos.]* **2002**, *107* (D5–D6), art. no. 4046.
- Davis, H. F.; et al. Dissociation energy and photochemistry of NO<sub>3</sub>. *J. Phys. Chem.* **1993**, *97* (10), 2172–2180.
- Johnston, H. S.; Davis, H. F.; Lee, Y. T. NO<sub>3</sub> photolysis product channels—quantum yields from observed energy thresholds. *J. Phys. Chem.* **1996**, *100* (12), 4713–4723.
- Orphal, J.; Fellows, C. E.; Flaud, P.-M. The visible absorption spectrum of NO<sub>3</sub> measured by high-resolution Fourier transform spectroscopy. *J. Geophys. Res.* **2003**, *108*, 4077–4087.
- Marinelli, W. J.; Swanson, D. M.; Johnston, H. S. Absorption cross sections and line shape for the NO<sub>3</sub> (0–0) band. *J. Chem. Phys.* **1982**, *76* (6), 2864–70.
- Ramsay, D. A. Optical spectra of gaseous free radicals. In *Proceedings of the Xth Colloquium Spectroscopium Internationale*; Lipincot, E. R., Margoshes, M., Eds.; Spartan Books: New York, 1963; pp 583–596.
- Douglas, A. E. Anomalous long radiative lifetimes of molecular excited states. *J. Chem. Phys.* **1966**, *45* (3), 1007–1015.
- Nelson, H. H.; Pasternack, L.; McDonald, J. R. Laser-induced excitation and emission spectra of NO<sub>3</sub>. *J. Phys. Chem.* **1983**, *87* (8), 1286–1288.
- Cleary, P. A.; Wooldridge, P. J.; Cohen, R. C. Laser-induced fluorescence detection of atmospheric NO<sub>2</sub> with a commercial diode laser and a supersonic expansion. *Appl. Opt.* **2002**, *41* (33), 6950–6956.
- Voigt, S.; Orphal, J.; Burrows, J. P. The temperature and pressure dependence of the absorption cross-sections of NO<sub>2</sub> in the 250–800 nm region measured by Fourier transform spectroscopy. *J. Photochem. Photobiol., A* **2002**, *149* (1–3), 1–7.
- Yokelson, R. J.; et al. Temperature Dependence of the NO<sub>3</sub> Absorption Spectrum. *J. Phys. Chem.* **1994**, *98* (50), 13144–13150.
- Patten, K. O.; Burley, J. D.; Johnston, H. S. Radiative lifetimes of nitrogen-dioxide for excitation wavelengths from 400 to 750 nm. *J. Phys. Chem.* **1990**, *94* (20), 7960–7969.
- Donnelly, V. M.; Keil, D. G.; Kaufman, F. Fluorescence lifetime studies of NO<sub>2</sub>. 3. Mechanism of fluorescence quenching. *J. Chem. Phys.* **1979**, *71* (2), 659–673.
- Clough, P. N.; Thrush, B. A. Mechanism of chemiluminescent reaction between nitric oxide and ozone. *Trans. Faraday Soc.* **1967**, *63* (532P), 915–925.
- Schurath, U.; Lippmann, H. H.; Jesser, B. Temperature-dependence of the chemi-luminescent reaction 1, NO + O<sub>3</sub> → NO<sub>2</sub>(<sup>2</sup>A<sub>1</sub> ← <sup>2</sup>B<sub>1,2</sub>) + O<sub>2</sub>, and quenching of the excited product. *Ber. Bunsen-Ges. Phys. Chem.* **1981**, *85* (9), 807–813.
- Sander, S. P.; et al. *Chemical Kinetics and Photochemical Data for Use in Atmospheric Studies*; JPL Publication 02-25; 2003; Evaluation No. 14.

- (40) Delon, A.; Jost, R.; Jacon, M. Laser induced dispersed fluorescence spectroscopy of 107 vibronic levels of NO<sub>2</sub> ranging from 12000 to 17600 cm<sup>-1</sup>. *J. Chem. Phys.* **2001**, *114* (1), 331–344.
- (41) Hard, T. M.; et al. Tropospheric free-radical determination by FAGE. *Environ. Sci. Technol.* **1984**, *18* (10), 768–777.
- (42) Holland, F.; Hessling, M.; Hofzumahaus, A. In situ measurement of tropospheric OH radicals by laser-induced fluorescence—a description of the Kfa instrument. *J. Atmos. Sci.* **1995**, *52* (19), 3393–3401.
- (43) Creasey, D. J.; et al. Implementation and initial deployment of a field instrument for measurement of OH and HO<sub>2</sub> in the troposphere by laser-induced fluorescence. *J. Chem. Soc. Faraday Trans.* **1997**, *93* (16), 2907–2913.
- (44) Kanaya, Y.; et al. Development of a ground-based LIF instrument for measuring HO<sub>x</sub> radicals: Instrumentation and calibrations. *J. Atmos. Chem.* **2001**, *38*, 73–110.
- (45) Wennberg, P. O.; et al. Removal of stratospheric O<sub>3</sub> by radicals—In-situ measurements of OH, HO<sub>2</sub>, NO, NO<sub>2</sub>, ClO, and BrO. *Science* **1994**, *266* (5184), 398–404.
- (46) Brune, W. H.; Anderson, J. G.; Chan, K. R. In situ observations of BrO over Antarctica—ER-2 aircraft results from 54-degrees-S to 72-degrees-S latitude. *J. Geophys. Res. [Atmos.]* **1989**, *94* (D14), 16639–16647.
- (47) Brune, W. H.; Anderson, J. G.; Chan, K. R. In situ observations of ClO in the Antarctic—ER-2 aircraft results from 54-degrees-S to 72-degrees-S latitude. *J. Geophys. Res. [Atmos.]* **1989**, *94* (D14), 16649–16663.

*Received for review May 20, 2003. Revised manuscript received September 22, 2003. Accepted September 30, 2003.*

ES034507W